Finite-size effects on acoustic phonons in GaAs/AlAs superlattices

M. Trigo and A. Fainstein*,†
Centro Atómico Bariloche and Instituto Balseiro, Comisión Nacional de Energía Atómica, 8400 San Carlos de Bariloche, Río Negro, Argentina

B. Jusserand and V. Thierry-Mieg
Laboratoire de Photonique et de Nanostructures, CNRS, Route de Nozay, 91460 Marcoussis, France
(Received 25 April 2002; published 24 September 2002)

We present a detailed study of the Raman-scattering spectra by acoustical phonons in finite-size GaAs/AlAs superlattices. The scattering geometry relies on an optical microcavity to enhance the Raman efficiency and to access the $q_z=0$ forward-scattering contribution. The results are analyzed using a photoelastic model for the Raman efficiency, which takes into account the superlattices finite size, the cavity confined optical field, and the acoustical-phonon displacements including the elastic modulation. The latter are derived from a matrix method implementation of the elastic continuum model for the complex layered structure. The calculations provide a complete description of the main experimental results that include: (i) the observation of low-energy oscillations, (ii) the presence of three main Raman lines in the first folded-phonon spectral region, (iii) the broadening of the Raman peaks, and (iv) the spectral shift of the lines with respect to the infinite superlattice. In addition, the observed asymmetry of the main central peak is understood as due to a q_z-nonconservation induced violation of the expected center-zone Raman selection rule. Besides providing a clear observation of the finite-size effects on superlattice acoustical phonons, the reported results demonstrate the use of microcavity geometries to access center-zone minigap excitation in layered structures.

DOI: 10.1103/PhysRevB.66.125311 PACS number(s): 78.30.Fs, 42.60.Da, 63.20.Dj, 78.66.Fd

I. MOTIVATION

Due to the spectral overlap and small elastic impedance mismatch, the acoustical-phonon branches in an ideal superlattice (SL) made up of a periodic sequence of semiconductor layers can be described by backfolding the phonon dispersion of an average bulk solid and opening of small minigaps at the zone center and reduced new Brillouin-zone edge.[1] On the other hand, in a Raman process performed in an infinite ideal SL in the transparency region crystal momentum is conserved. For a backscattering geometry along the growth direction this implies that the wave vector transferred is $q_z=k_L+k_S$, with $k_L(k_S)$ the laser (scattered) wave number. Thus, in a Raman-scattering experiment involving longitudinal-acoustic (LA) phonons, characteristic doublets that reflect the folding of the phonon dispersion are observed.[1]

The above picture changes in *finite* SL's made by only a few periods, for which Brillouin-zone schemes and crystal momentum conservation do not hold. Finite semiconductor heterostructures have been investigated for some time.[2–11] From the experimental point of view, the finite-size effects have been identified in different kinds of excitations. These include plasmons in multilayers with two-dimensional electron gases,[5] optical phonons in GaAs/AlAs multiple quantum wells,[7,8] and acoustical phonons in semiconductor superlattices.[9–11] Plasmons and optical phonons are excitations confined to specific layers, which are coupled through long-range Coulomb interactions. The observed effects may be basically resumed in the apparition of ''surface modes'' at the limiting surfaces of the sample, and in a discretization of the wave vector along the heterostructure growth axis (z). Also, a relaxation of the wave vector conservation along z is observed in the Raman-scattering process.[5–7] Standing optical vibrations have also been recently reported.[8] Acoustical phonons are different as the interactions are short range but the excitations extend throughout the structure. The finite-size effects reported in the literature include standing acoustical waves of the whole structure[9,10] and interference effects in Raman scattering observed in so-called mirror-plane superlattices.[11]

In this paper, we report on an experimental and theoretical investigation of finite-size effects on Raman scattering in GaAs/AlAs SL's made by only a few periods. In order to enhance the weak Raman efficiency, we use a coupled optical microcavity designed for Raman double optical resonance studies. The microcavity consists of two identical GaAs/AlAs SL's forming, respectively, the spacer of two coupled microcavities, and which are separated and cladded by distributed Bragg reflectors (DBR's).[8] The structure has two optical modes that can be used for optical resonance enhancement.[6] We address issues concerning the SL's limited number of periods, the coupling between the two SL's, and the implication of photon confinement in the Raman-scattering process. We show that several interesting effects arise and that a photoelastic model including the proper description of the structure's acoustical vibrations and photon field provide a precise quantitative description of the Raman-scattering spectra.

The paper is organized as follows. In the following section, we describe the coupled optical microcavity sample and the Raman scattering setup used for double optical resonance amplification. In Sec. III, we present and discuss the experimental results and calculations. Finally, some conclusions are drawn in Sec. IV, and implications for the manipulation of acoustical excitations and their study in optically confined structures are presented.

II. SAMPLE AND EXPERIMENTAL SETUP

Semiconductor planar optical microcavities are dielectric layered structures consisting of the optically active medium enclosed by DBR's.[12,13] In these photonic structures the optical field is confined and enhanced within the active region, leading to a variety of phenomena that include a modified emission rate and strongly coupled exciton-cavity-photon polaritons.[12] It has been shown[6,13–15] that the cavity modified photon spectral and spatial density of states can be used to enhance the inelastic light-scattering efficiency with amplification factors $\sim 10^4 - 10^5$.

In standard microcavities designed with only one confined optical mode, the tuning of both the laser and the Stokes (nondegenerate) photons can be accomplished by tuning the incidence and scattered angles with respect to the growth axis (z).[6,14,16] This scattering geometry is appropriate for the study of small energy excitations, but becomes cumbersome above ~ 35 meV (e.g., for optical phonons) where incidence angles typically larger than $\sim 50°$ have to be used. In this latter case, more convenient microcavities with two optical modes can be designed.[8,17,18] These coupled double microcavities consist of two $\lambda/2$ spacers enclosed by top and bottom DBR's, and separated by a lower reflectivity mirror. Two split cavity modes exist with maxima in the spacers. But the two modes differ in their parity (symmetric and antisymmetric) with respect to the center of the structure.[19]

A coupled cavity designed as described above was used in Ref. 8 to study the optical phonons of finite SL's. This same structure will be used here for investigating the Raman-scattering acoustical-phonon spectra of finite SL's in a microcavity geometry. Since the acoustical-folded-phononlike excitations are in the range 10–30 cm^{-1} (i.e., $\sim 1 - 4$ meV), the angular tuning of the double optical resonance using a single cavity mode[6,14,16] is straightforward and thus a coupled double microcavity is not required for this purpose. However, the sample has the added interest of the phonon-coupling effects between SL's and the possibility to perform the Raman process through either one of the symmetric or the antisymmetric cavity modes. These two issues will be considered in this work besides the results intrinsic to the individual SL's finite size. In our experiments, for Stokes (anti-Stokes) spectra the collection (excitation) was set along *z*, while the excitation (collection) angle was adjusted around $\sim 3° - 5°$ for double optical resonant enhancement using either one of the two cavity modes.

The studied structure consists of two $\lambda/2$ spacers made by 10.5-period GaAs(8.5 nm)/AlAs(4.4 nm) SL's of 8.5-nm/4.4-nm nominal width. These spacers were enclosed by 20 DBR $Ga_{0.8}Al_{0.2}As$/AlAs pairs on the bottom, 16 on top, and 8.5 in between. The structure was purposely grown with a slight taper that enables a tuning of the cavity modes by displacing the laser spot on the sample surface (see Fig. 1 of Ref. 8). The two cavity modes, split by ~ 35 meV, can be tuned this way from ~ 1.45 eV (855 nm) to ~ 1.55 eV (800 nm). The layer widths at the precise spot where the Raman spectra were acquired were deduced from the total cavity width as derived from the cavity mode energy, assuming that the nominal GaAs/AlAs width ratio is constant throughout the whole structure.

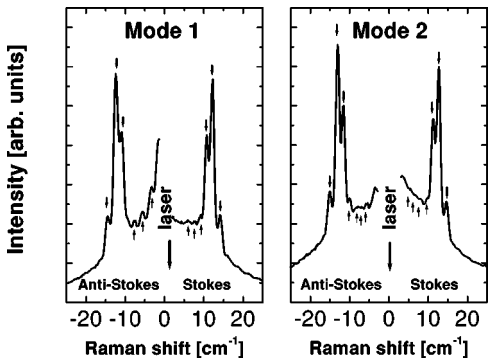

FIG. 1. Typical Stokes and anti-Stokes spectra in the energy region corresponding to the first folded-acoustic phonons, obtained with 850-nm excitation using either the upper (1) or lower (2) cavity mode for Raman amplification.

The Raman experiments were performed at 77 K using a triple Jobin-Yvon *T*64000 spectrometer equipped with a N_2-cooled charge-coupled device. A Ti-sapphire laser was used as the excitation source at energies in the range 810–850 nm, well below the SL's fundamental exciton absorption (~ 1.6 eV$=775$ nm). Due to some weak parasitic luminescence coming from the substrate, the best spectra were obtained at ~ 850 nm, below the GaAs gap (1.515 eV$=820$ nm). The spectra were acquired using a triple subtractive configuration with spectral resolution around 0.1–0.2 cm^{-1}.

III. RESULTS

In this section, we will present the experimental results and calculations based on a photoelastic model for the Raman-scattering efficiency. In order to separate the effects that are due exclusively to interference properties of the Raman efficiency[11] from those that essentially depend on the acoustic-phonon structure of the finite SL's, calculations have been performed both considering the bulklike acoustic phonons of an average medium, and also the appropriate solution of the acoustic wave equation in the layered medium. We will address the following issues: (i) the finite-size effects in the Raman spectra, that is, phenomena due to the reduced number of SL layers, (ii) consequences in the scattering process due to the cavity-photon confinement, (iii) coupling effects between the two SL's, and, last, (iv) whether the symmetry of the photon cavity mode is relevant or not for the Raman process. The section is organized as follows: we first present the experimental results, followed by calculations that enable a separate description of the observed effects, and finally by a discussion in which the full calculation is compared with the experimental results.

A. Experiment

In Fig. 1, we show typical spectra obtained with 850-nm excitation using either the upper or lower cavity mode for Raman amplification. Such cavity tuning was accomplished by displacing the laser spot in the sample surface while keep-

ing all other experimental parameters fixed. The cavity mode linewidth, determined mainly by the collection solid angle and the laser spot diameter, was around 10–12 cm^{-1}. This implies that no peak is selectively amplified, and thus that the relative intensity of the different spectral features is intrinsic.[6,14]

The most important results are as follows:

(i) three main peaks are observed at $\sim 10.9\ cm^{-1}$, $\sim 12.4\ cm^{-1}$, and $\sim 14.5\ cm^{-1}$, respectively. These are labeled with thick down arrows in Fig. 1. The doublet expected assuming a standard backscattering spectra with 850-nm excitation should be split by $\sim 2.8\ cm^{-1}$. Note, however, that the full separation of these peaks is $\sim 3.6\ cm^{-1}$ and that no pair can be assigned straightforwardly to the first folded-acoustic-phonon doublet.

(ii) Besides the main peaks, weaker equally spaced oscillations are well discerned mainly towards low energies (indicated with up arrows in Fig. 1). Note in particular the anti-Stokes spectrum of mode 1, which was taken with the Raman amplification set at lower energies in order to highlight these features.

(iii) The peaks in the spectra are relatively broad. The linewidth is intrinsic as verified by increasing the spectral resolution with no noticeable change in the spectral shape.

(iv) The spectra taken with mode 1 and 2 are similar, indicating that the symmetry of the cavity mode is not relevant to the Raman-scattering process.

B. Photoelastic model calculations

Within a photoelastic model for scattering by longitudinal-acoustic phonons the Raman efficiency is given by[1]

$$I(\omega_{q_z}) \propto \left| \int dz E_L E_S^* p(z) \frac{\partial \Phi(z)}{\partial z} \right|^2, \qquad (1)$$

where $E_L(E_S)$ is the laser(scattered) field, $p(z)$ is the spatially varying photoelastic constant, and Φ describes the phonon displacement. For an infinite periodic SL, the wave vector q_z is a good quantum number for the structure's vibrations. In this case and for the usual experimental conditions given by a backscattering geometry with laser and the scattered fields given by plane waves ($E_L E_S^* = e^{i(k_L + k_S)z}$), Eq. (1) leads to the phonon doublets with transferred wavenumber given by the conservation law $q_z = k_L + k_S$. For the case we are discussing, however, the following points must be considered: (i) the integration is performed for limited values of z given by the finite size of the structure, (ii) E_L and E_S correspond to the cavity confined photons and their amplitude and spatial distribution have to be properly taken into account, and (iii) in order to fully describe the Raman spectra the phonon-displacement pattern Φ has to be evaluated considering the acoustic modulation of the real structure.[1]

For the evaluation of the acoustical phonons in the layered structure, we have used the standard elastic continuum description of the sound waves as originally proposed by Rytov[20] and implemented using a matrix method by He and co-workers.[21] With this model one can obtain the transmission of acoustical waves through the structure, and the displacement pattern as a function of the phonon energy, which is used as input for the evaluation of the Raman efficiency [Eq. 1]. The matrix method is equivalent to that used to describe the propagation of light in layered media,[22] and which we implemented for the calculation of the cavity photon field. In order to discern the interference effects that arise from the photoacoustic modulation of the finite structure[11] from those effects that reflect the specific phonon pattern of the acoustically modulated structure, we compare the results with calculations of the Raman efficiency using a simplified average medium description of the phonon spectra. Within this latter description the phonon displacement pattern is taken as $\Phi(z) = \cos(q_z z)$, with the dispersion relation given by $\omega_q = |q_z| v_{ac}$ with v_{ac} the average sound velocity.[1,11] We note that such a linear dispersion does not include the folded-phonon minigaps and thus is strictly valid only away from the reduced Brillouin-zone edges.

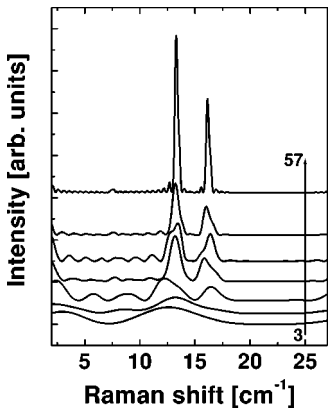

FIG. 2. Calculated Raman spectra for GaAs/AlAs SL's of varying number of layers from 3 to 57. The GaAs/AlAs layer widths are constant and correspond to the real structure (74 Å/38 Å).

In Fig. 2, we show calculated Raman spectra in the spectral region corresponding to the first folded-phonon doublet and for GaAs/AlAs SL's of varying number of periods from 1.5 to 28.5. The GaAs/AlAs layer widths are constant and correspond to the real structure (74 Å/38 Å), as determined from the nominal GaAs/AlAs ratio and the cavity mode energy at the specific sample spot where the Raman amplification was performed. For the shown spectra we consider a single SL and a standard backscattering configuration with $\lambda = 850$ nm. Note that quasiconservation of wave vector leads to the observation of doubletlike features for as few as 3.5 SL periods (third curve from bottom). The finite-size effects are apparent in the spectra, including the broadening of the peaks and the observation of oscillations in the low-energy side of the doublet. These features are conceptually similar to a diffraction pattern where the peak widths depend on the number of illuminated grooves and the satellites correspond to the side maxima.[11] Note also that these oscillations modulate the whole spectra. In consequence, the precise position of the doubletlike peaks is size dependent, this effect being clearer for the structures with fewer periods and hence broader spectra.

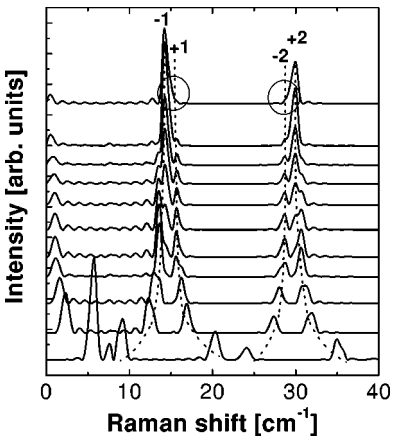

FIG. 3. Calculated Raman spectra for a single SL with parameters of the real structure (actual number of periods and layer widths) as a function of transferred q_z and for a standard backscattering geometry. The transferred wave vector spans the range from $q_z=0$ (top spectrum) to $q=211\times10^4$ cm^{-1} (bottom-most spectrum). The spectral region corresponding to the first two folded-phonon doublets (±1 and ±2) is shown. The dotted curves are guides to the eye. Note that the $q_z=0$ peaks are asymmetric, with nonzero scattering weight at the position of the ''forbidden'' doublet modes [$(+1)$ for the $\sim$15-cm^{-1} doublet and (-2) for the $\sim$30-cm^{-1} one]. The latter are highlighted with circles in the figure.

Another interesting feature deriving from the SL finite size can be appreciated in Fig. 3, where we present calculated Raman spectra for a single SL with the real structure (actual number of periods and layer widths) as a function of transferred q_z and for a standard backscattering geometry. The transferred wave vector spans the range from $q_z=0$ (top spectrum) to $q=211\times10^4$ cm^{-1} (bottom-most spectrum). The latter corresponds to a laser wavelength $\lambda=200$ nm with an effective refractive index of the SL's, $n_{eff}=3.36$. The spectral region corresponding to the first two folded-phonon doublets is shown. The position of the doublet peaks basically reflects the q_z dispersion of the acoustical phonons of an infinite SL with the same period and GaAs/AlAs ratio. Note that while two doublet peaks are observed for large q_z's, only one is apparent for $q_z=0$. For an infinite SL and $q_z=0$, the two phonon modes corresponding to the center-zone doublets differ in their parity with respect to the center of the layers.[1] This leads, following Eq. (1), to one of these modes being Raman forbidden. Interestingly, note that for our finite-size structure q_z conservation is partially relaxed leading to a ''violation'' of this selection rule. This is reflected, in the shown calculated spectra, in asymmetric peaks for $q_z=0$ with nonzero scattering weight at the position of the ''forbidden'' peak [$(+1)$ for the $\sim$15-cm^{-1} doublet and (-2) for the $\sim$30-cm^{-1} one].

The above discussed figures were obtained considering the standard backscattering geometry with laser and scattered fields described by plane waves. When the SL is embedded in a microcavity and under double optical resonance conditions, on the other hand, both the laser and the Stokes fields correspond to cavity confined modes. In this case within the spacer the z dependence of the two photon fields are given by

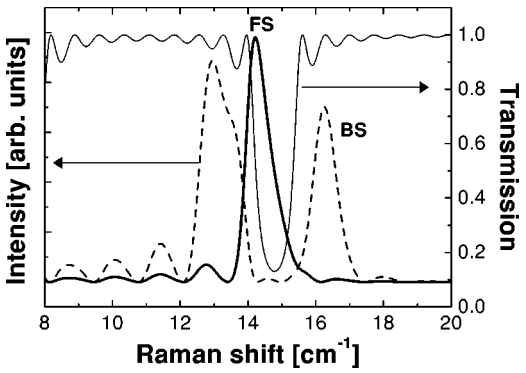

FIG. 4. Calculated forward-scattering (FS, solid thick curve) and backscattering (BS, dashed curve) contribution to the $\lambda=850$-nm Raman spectra corresponding to a single 10.5-period SL embedded in a microcavity. The spectra are superimposed to the phonon transmission amplitude in the first folded-phonon doublet energy region (see text for details).

the same standing wave $E_L=E_S=e^{ik_zz}+e^{-ik_zz}$, where, by construction, $k_z=\pi/D$ (D is the spacer width).[8] Note that the laser and the Stokes photons are tuned with the same cavity mode but slightly different angles, that is, different $k_\parallel$. In consequence, in Eq. (1) the photon field part of the integrand is given, besides a multiplicative constant determined by the amplification characteristics of the cavity, by[8]

$$E_LE_S^*=|E(z)|^2=2+(e^{i2k_zz}+e^{-i2k_zz}). \tag{2}$$

Equation (2) implies, on one hand, that the Raman efficiency is exactly the same whether the experiment is performed through any one of the two cavity modes, in correspondence with the experimental results. On the other hand, it indicates that, in a cavity, both a forward-scattering (the term 2) and a backscattering contribution ($e^{i2k_zz}+e^{-i2k_zz}$) are coherently added to the Raman efficiency. The former corresponds to a wave-vector transfer $q_z=0$, while for the latter $q_z=2\pi/D$.

We show in Fig. 4 calculated $\lambda=850$-nm Raman spectra corresponding to a single 10.5-period SL embedded in a microcavity where, for clarity, we have evaluated separately the forward-scattering and backscattering terms. The shown spectra correspond to the first folded-phonon doublet region, and are superimposed to the phonon transmission amplitude calculated with the matrix method discussed above. Several features should be highlighted:

(i) the transmission minimum corresponds to the first center-zone minigap.

(ii) The backscattering doublet is centered at this minigap, and displays the discussed low-energy oscillations and the Raman selection rule which explains the stronger intensity of the (-1) peak. These peaks are out of the minigap because $q_z\neq0$.

(iii) The forward-scattering peak corresponds to $q_z=0$ and thus appears at the low-energy limit of the minigap. Note that, as discussed above, due to partial q_z nonconservation this latter peak is asymmetric with nonzero scattering weight

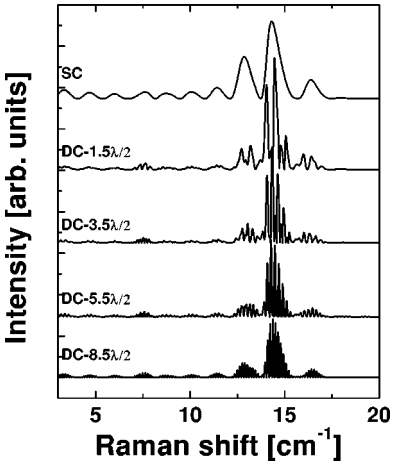

FIG. 5. Raman spectra calculated for two 10.5-period SL's embedded in double microcavities with varying number of intermediate DBR layers. For comparison we also show the spectrum of a single SL in a cavity (topmost curve). The SL parameters are those of our real structure.

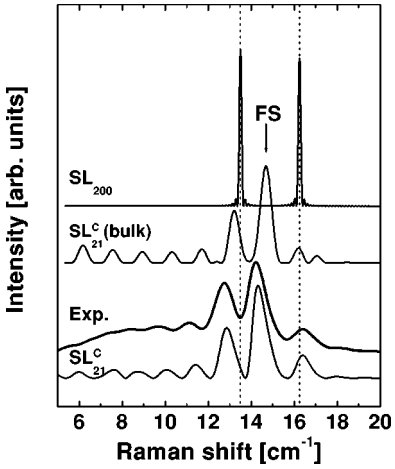

FIG. 6. We show from top to bottom: (i) a calculated spectrum corresponding to an ''infinite'' SL made by 100 periods and a backscattering standard configuration (SL_{200}), (ii) spectrum of a single SL in a microcavity calculated considering the linear average media acoustical-phonon dispersion (SL^{C}_{21}(bulk)), (iii) a typical experimental curve (Exp.), and (iv) the full calculation for a microcavity embedded SL with phonon modes derived including the acoustical modulation (SL^{C}_{21}). In all cases $\lambda = 850$ nm. FS labels the forward-scattering contribution.

within the gap and at the high-energy side of the minigap. The high-energy side corresponds to the ''forbidden'' $(+1)$ term.

(iv) The low-energy oscillations add coherently from the backscattering and forward-scattering contributions, thus explaining their strong intensity in the experimental spectra.

The observation of forward scattering due to the cavity confinement deserves a brief comment. In fact, although it is customary to assume in Raman scattering in bulk materials that the transferred wave vector is almost zero in comparison to the bulk Brillouin-zone edge ($4\pi/\lambda \ll \pi/a$, with λ the laser wavelength and a the lattice parameter), it is nonnegligible in terms of the reduced SL Brillouin zone. Consequently, the observed Raman doublets typically reflect the bulk dispersion folding but are not influenced by the opening of the minigaps. In order to probe the minigaps, two strategies have been pursued in the literature. On one hand, the zone edge can be sensed by a proper design of the SL structures.[23,24] On the other hand, forward-scattering geometries have been used.[25] As follows from Fig. 4, the cavity geometry provides direct access to the minigap modes. In addition, in finite-size structures q_z nonconservation leads to spectral weight within the minigap energy range. As we will discuss below, this result may have interesting implications for the study of acoustically confined structures.

Having discussed the effect of the SL finite size and of the cavity confinement, we address next the implications of having two separate SL, coupled through the intermediate DBR mirror. In Fig. 5, we show Raman spectra calculated for two 10.5-period SL's embedded in double microcavities with varying number of intermediate DBR layers. For comparison we also show the spectrum of a *single* SL in a cavity (topmost curve). In all cases the SL parameters are those of our real structure. The bottom-most spectrum, with $8.5\lambda/2$ DBR layers, corresponds to the double cavity used in our experiments. As it is apparent from the spectra, the coupling of the two SL's leads to a rapid modulation of spectra with basically the same envelope function. This modulation reflects two different physical phenomena: first, an interference of the scattered field coming from the two SL's. These features are also present in calculations performed with the phonon field described by a linear average media dispersion. Such ''interference effect'' is similar to that described for the ''mirror-plane'' superlattices reported in Ref. 11. And second, scattering intensities that depend on the phonon displacement of acoustical modes that are specific to the complex layered structure. The weight of the phonon pattern at the SL's, and the symmetry of the displacements within each SL layer, basically determine the Raman efficiency for that specific mode. In any case, for the studied structure this modulation is below the resolution limit of the experimental setup, and thus we can conclude that the observed spectra essentially reflect the properties of the envelope function, that is, the spectrum of a single-cavity confined finite-size SL.

C. Discussion

We now proceed to compare the experimental Raman spectra of our double finite SL structure embedded in a cavity with the photoelastic model calculations. For that purpose we show in Fig. 6 from top to bottom: (i) a calculated spectrum corresponding to an ''infinite'' SL made by 100 periods and a backscattering standard configuration; (ii) a single SL in a microcavity calculated considering the linear average media acoustical-phonon dispersion; (iii) a typical experimental curve; and (iv) the full calculation for a microcavity embedded SL with phonon modes derived including the acoustical modulation. In all cases $\lambda = 850$ nm.

The ''infinte'' SL curve (SL_{200}) defines the standard spectrum with two narrow doublet peaks separated by ~ 2.8 cm^{-1}. The (-1) component is slightly stronger due to the discussed parity Raman selection rule. The compact

weak oscillations are discernible close to the major peaks much like in a diffraction grating pattern. The cavity spectrum calculated with average ''bulklike'' phonons [SL_{21}^{C} (bulk)], on the other hand, helps to identify those features that derive solely from (1) the interferences in the Raman cross section due to the SL's finite size, and (2) from the cavity photon confinement (effects due to the real phonon structure only appear when the acoustical modulation is fully taken into account and will be discussed below). First, the peaks are broader as expected from a diffractionlike pattern with fewer source layers. Concomitant with this, low-energy side oscillations appear as in the experimental spectra. In addition, the backscattering maxima are shifted with respect to the infinite SL doublet position as in the experimental data, although a quantitative agreement for the peak positions is not obtained. This line shift is a consequence of the finite-size originated oscillatory modulation of the doublet-like broad peaks. Finally, a forward-scattering peak is observed between the backscattering doublet. Note that there is a single peak centered with respect to the doublet because the ''bulklike'' phonon dispersion does not include the minigaps originated in the acoustical modulation. This contrasts with the experimental curve where clearly an asymmetric noncentered peak is observed. In any case the simplified model with the bulklike phonons accounts for many of the experimental results, including the presence of three main peaks, the broadening of the peaks, the increase of the doublet separation, and the existence of low-energy oscillations.

The asymmetry and shift of the central forward-scattering contribution is an important point that requires further discussion. In fact, this feature can be fully accounted for when the proper description of the phonon spectra (that is, including the acoustical modulation) is taken into account. Such calculation is displayed as the bottom-most spectrum in Fig. 6 (curve SL_{21}^{C}). As discussed extensively in Sec. II B, for an infinite superlattice and due to a parity selection rule, the $q_z=0$ spectra display only one component of the center-zone doublet. For $q_z\neq 0$, on the other hand, this selection rule is partially relaxed and the two components of the doublet are observed, their splitting and relative intensity varying with the transferred wave vector (see Fig. 3). Consequently, in a *finite*-size SL, q_z partial nonconservation leads to the observation of the ''forbidden'' component of the doublet in the forward-scattering $(q_z=0)$ contribution. This explains the observed asymmetry of the main peak at $\sim 14.5\ cm^{-1}$. For the backscattering part, on the other hand, wave vector nonconservation basically leads only to a line broadening. Note in Fig. 6 that when the full calculation including the acoustical modulation is considered, the agreement with the experiment is remarkable without any adjustable parameter. This includes the features described above for the simpler average media model, but also almost every other detail of the experimental results: the existence of three main peaks, the asymmetry of the forward-scattering contribution, the appearance of oscillations and their period, the spectral position and relative intensity of all peaks (including the weak peak at $\sim 18\ cm^{-1}$), and the line widths.

IV. CONCLUSIONS

We have presented a detailed experimental and theoretical study of GaAs/AlAs superlattice Raman spectra in microcavity confined geometries. This allowed us to study the finite-size effects on the acoustical-phonon spectra, and demonstrated the strength of the matrix method implementation of the standard photoelastic model with an elastic continuum description of the vibrations to fully describe the experimental results. Most interestingly, we showed that the photon confinement provides a natural way to access $q_z=0$ excitation which, in this case, correspond to the folded-phonon minigap modes. In addition, due to q_z nonconservation in the finite SL, Raman-scattering from the otherwise forbidden component of the phonon doublet and from modes within the minigap become observable. We believe that this is an interesting result that opens the way to the study of modulated structures with confined acoustical vibrations. In fact, as the dielectric modulation of the DBR's results in the appearance of ''photon gaps,'' the acoustical modulation opens the phonon minigaps that act as mirrors for sound waves.[26] Extending the idea of the photon microcavities we can thus conceive ''phonon cavities'' made by a spacer enclosed by appropriately designed SL's acting as phonon DBR's. The consequence would be the appearance of phonon confined modes with energies within the folded-phonon minigap, and with the displacement patterns localized within the central spacer. Such novel ''confined acoustical phonons'' could be spectrally accessible with Raman experiments similar to the ones described in this work. These experiments are under way and will be the subject of future work.

*Email address: afains@cab.cnea.gov.ar
†Also at CONICET, Argentina.

[1] B. Jusserand and M. Cardona, in *Light Scattering in Solids V,* edited by M. Cardona and G. Güntherodt (Springer, Heidelberg, 1989), p. 49.
[2] R.E. Camley and D.L. Mills, Phys. Rev. B **29**, 1695 (1984).
[3] P. Hawrylak, G. Eliasson, and J.J. Quinn, Phys. Rev. B **34**, 5368 (1986).
[4] J.K. Jain and P.B. Allen, Phys. Rev. Lett. **54**, 947 (1985); **54**, 2437 (1985).
[5] A. Pinczuk, M.G. Lamont, and A.C. Gossard, Phys. Rev. Lett. **56**, 2092 (1986).
[6] A. Fainstein, B. Jusserand, and V. Thierry-Mieg, Phys. Rev. Lett. **75**, 3764 (1995).
[7] A. Fainstein and B. Jusserand, Phys. Rev. B **54**, 11 505 (1996).
[8] A. Fainstein, M. Trigo, D. Oliva, B. Jusserand, T. Freixanet, and V. Thierry-Mieg, Phys. Rev. Lett. **86**, 3411 (2001).
[9] P.X. Zhang, D.J. Lockwood, and J.-M. Baribeau, Can. J. Phys. **70**, 843 (1992).
[10] A. Mlayah, R. Grac, G. Armelles, R. Carles, A. Zwick, and F. Briones, Phys. Rev. Lett. **78**, 4119 (1997).
[11] M. Giehler, T. Ruf, M. Cardona, and K. Ploog, Phys. Rev. B **55**, 7124 (1997).
[12] *Confined Electrons and Photons: New Physics and Applications,*

edited by E. Burstein and C. Weisbuch (Plenum, New York, 1995).
[13] M.S. Skolnick, T.A. Fisher, and D.M. Whittaker, Semicond. Sci. Technol. **13**, 645 (1998).
[14] T. Kipp, L. Rolf, C. Schüller, D. Endler, Ch. Heyn, and D. Heitmann, Phys. Rev. B **63**, 195304 (2001).
[15] B. Jusserand and A. Fainstein, in *Raman Scattering in Material Science*, edited by R. Merlin and B. Weber, Vol. 42 of Springer Series in Materials Science (Springer, Berlin, 2000).
[16] A. Fainstein, B. Jusserand, and V. Thierry-Mieg, Phys. Rev. B **53**, R13287 (1996); A. Fainstein and B. Jusserand, *ibid.* **57**, 2402 (1998).
[17] P. Pellandini, R.P. Stanley, R. Houdré, U. Oesterle, and M. Ilegems, Appl. Phys. Lett. **71**, 864 (1997).
[18] B. Jusserand, T. Freixanet, and A. Fainstein, Physica E (Amsterdam) **7**, 646 (2000).
[19] A. Armitage, M.S. Skolnick, V.N. Astratov, D.M. Whittaker, G. Panzarini, L.C. Andreani, T.A. Fischer, J.S. Roberts, A.V. Kavokin, M.A. Kaliteevski, and M.R. Vladimirova, Phys. Rev. B **57**, 14877 (1998).
[20] S.M. Rytov, Akust. Zh. **2**, 71 (1956).
[21] J. He, B. Djafari-Rouhani, and J. Sapriel, Phys. Rev. B **37**, 4086 (1988).
[22] A. Yariv and P. Yeh, *Optical Waves in Crystals* (Wiley, New York, 1984).
[23] J. He, J. Sapriel, J. Chavignon, R. Azoulay, L. Dugrand, F. Mollot, B. Djafari-Rouhani, and R. Vacher, J. Phys. (Paris) **48-C5**, 573 (1987).
[24] H. Brugger, H. Reiner, G. Abstraiter, H. Jorke, H.J. Herzog, and E. Kasper, Superlattices Microstruct. **2**, 451 (1986).
[25] B. Jusserand, F. Mollot, and D. Paquet, Surf. Sci. **228**, 151 (1990).
[26] V. Narayanamurti, H.L. Störmer, M.A. Chin, A.C. Gossard, and W. Wiegmann, Phys. Rev. Lett. **43**, 2012 (1979).